

### **Supplementary Figure 1 AAV6 variants show superior transduction efficiencies in human primary T cells**

- (a) An overview of the top AAV6 variants and wild-type AAV6 in the results of capsid screening.
- (b) The packing efficiencies of AAV6-WT, AAV6-M1, and AAV6-M2 using adherent HEK 293T cells in a 15 cm plate.
- (c) The packing efficiencies of AAV6-WT and AAV6-M2 using suspension HEK293 cells in a 3-liter bioreactor.
- (d) AAV6-M2 capsid content determined by analytic ultracentrifugation (AUC) at wavelength 280 nm.
- (e) Cropped view of a representative cryo-EM micrograph for AAV6-M2 sample.

### **Supplementary Figure 2 CD62L mediates enhanced transduction of AAV6-M2 in human T cells**

- (a) Volcano plots of genome-wide CRISPR screen hits for AAV6-M1, showing MAGeCK score versus log-fold change (LFC). Top-ranked candidates are highlighted.
- (b) Flow cytometry analysis of EGFP<sup>+</sup> in CD62L<sup>+</sup> and CD62L<sup>-</sup> human primary T cells transduced with AAV6-M2 and AAV6-WT. Data collected from T cells of three donors and CD62L-knockout by two independent sgRNAs.
- (c) Flow cytometry analysis of EGFP<sup>+</sup> in Jurkat cells 48 hours after AAV6-M2 transduction (MOI = 50). Three Jurkat cell populations were analyzed: non-targeting control knockout cells, CD62L knockout cells, and CD62L knockout cells complemented by CD62L overexpression.
- (d) Cryo-EM data processing workflow for AAV6-M2 capsid reconstruction.
- (e) Cryo-EM structure of the AAV6-M2 monomer shown in two orientations rotated 180°, highlighting the engineered VRVIII loop in orange.
- (f) Structural alignment of AAV6-WT (purple, PDB: 4V86) and AAV6-M2 (orange, PDB: 9VI4) VP3 monomers.

(g-h) Cryo-EM density maps (grey mesh) of the VRVIII loop fitted with atomic models from AAV6-M2 (f, yellow sticks) and AAV6-WT (g, purple sticks).

(i) Flow cytometry analysis of EGFP<sup>+</sup> human aT cells 24 hours after AAV6-M2 transduction (MOI = 1E4). In AAV6-M2-mut1, AAV6-M2-mut2, and AAV6-M2-mut3, residues E590, E591, and E592 were individually mutated to alanine, respectively. In AAV6-M2-mut4, all three residues (E590, E591, and E592) were simultaneously mutated to alanine.

(j) Schematic of serum susceptibility experiment.

### **Supplementary Figure 3 Efficient transduction and cytotoxicity of AAV6-M2-mediated CAR delivery in human T cells**

(a) Schematic of AAV6-M2-CAR vector and experimental timeline for transducing activated human primary T cells (aT), followed by flow cytometry analysis.

(b) Expansion of aT cells from two donors after transduction with AAV6-M2-CAR or no-AAV control.

(c) Time course of NALM6 cell elimination in cytotoxicity assays using AAV6-M2-CAR or AAV6-WT-CAR transduced aT cells (T:B = 1:1).

(d) Schematic of AAV6-M2-EGFP transduction in resting human T cells (rT), followed by flow cytometry analysis.

(e) Schematic of AAV6-M2-EGFP transduction in resting human T cells (rT) then CD3/CD28 beads activation, followed by flow cytometry analysis.

(f) Transduction efficiencies of AAV6-M2-EGFP in CD4<sup>+</sup> and CD8<sup>+</sup> T cells analyzed from non-activated human PBMC (n=4).

(g-h) Cytotoxicity in TCM (g) and TEM (h) cells over time following AAV6-M2-CAR transduction and NALM6 co-culture.

(i-k) Composition of T cell subsets over time in Tn (i), TCM (j), and TEM (k) populations post co-culture with NALM6 cells.

#### **Supplementary Figure 4 In vivo CAR-T cell generation and B cell depletion by AAV6-M2 in humanized mice**

(a-b) Frequencies of B cells and T cells in peripheral blood prior to AAV injection show no differences between treatment groups.

(c-d) Longitudinal dynamics of B cells in peripheral blood over 6 weeks.

(e) CAR<sup>+</sup> CD4<sup>+</sup> T cell frequencies in mouse tissues following AAV6-M2-CAR and AAV6-WT-CAR administration.

(f-i) Subset analysis of CAR<sup>+</sup> T cells across bone marrow (f), spleen (g), liver (h), and lung (i).

Each dot represents an animal. Data shown as mean  $\pm$  SEM; P values were calculated by unpaired T tests. P values were calculated by unpaired T tests; Statistical significance levels were not calculated for data in Week 6 due to limited available data points.

\*  $p \leq 0.05$ ; \*\*  $p \leq 0.01$ ; \*\*\*  $p \leq 0.001$ ; \*\*\*\*  $p \leq 0.0001$ .

#### **Supplementary Figure 5 AAV6-M2 in vivo CAR-T therapy eliminates B cells and ameliorates SLE symptoms in a humanized lupus model**

(a-d) hCD45<sup>+</sup> cells (a), total IgG (b), B cell counts (c), and anti-dsDNA levels (d) in peripheral blood prior to AAV injection.

(e) Percentage of B cells among hCD45<sup>+</sup> cells in multiple tissues.

(f) Composition of B cell subsets in bone marrow from one representative mouse.

(g-j) Quantification of transitional (g), naïve (h), memory (i), and plasmablast B cells (j) in bone marrow.

(k-l) Plasmablast and plasma cell (PB & PC) abundance in the spleen quantified by flow cytometry (k) and flow cytometry contour plot (l).

(m) Representative kidney immunofluorescence images showing reduced human IgG deposition in AAV-treated mice. This plot is associated with Figure 5e.

(n–o) Quantification of B cells (n) and histological analysis (o) in the lung. This plot is associated with Figure 5j.

(p–q) Quantification of B cells (p) and histological analysis (q) in the liver. Yellow arrows indicate immune cells infiltrated into the liver.

Each dot represents an animal. Data shown as mean  $\pm$  SEM; P values were calculated by unpaired T tests.

\*  $p \leq 0.05$ ; \*\*  $p \leq 0.01$ ; \*\*\*  $p \leq 0.001$ ; \*\*\*\*  $p \leq 0.0001$ ; ns: not significant.

### **Supplementary Figure 6 Vector liver accumulation**

(a) The viral copy numbers in the isolated human T cells from the spleen of HIS mouse 12 hours post AAV6-M2 injection ( $3 \times 10^{13}$  vg/kg).

(b) Surface charges are displayed for AAV6-WT and AAV6-M2. blue: positive; red: negative.

(c) qPCR quantification of viral copies in the liver of B6 mice 10 days post scAAV-EGFP injection ( $5 \times 10^{12}$  vg/kg).

(d) Quantification of EGFP signals in the liver of B6 mice 10 days post scAAV-EGFP injection.

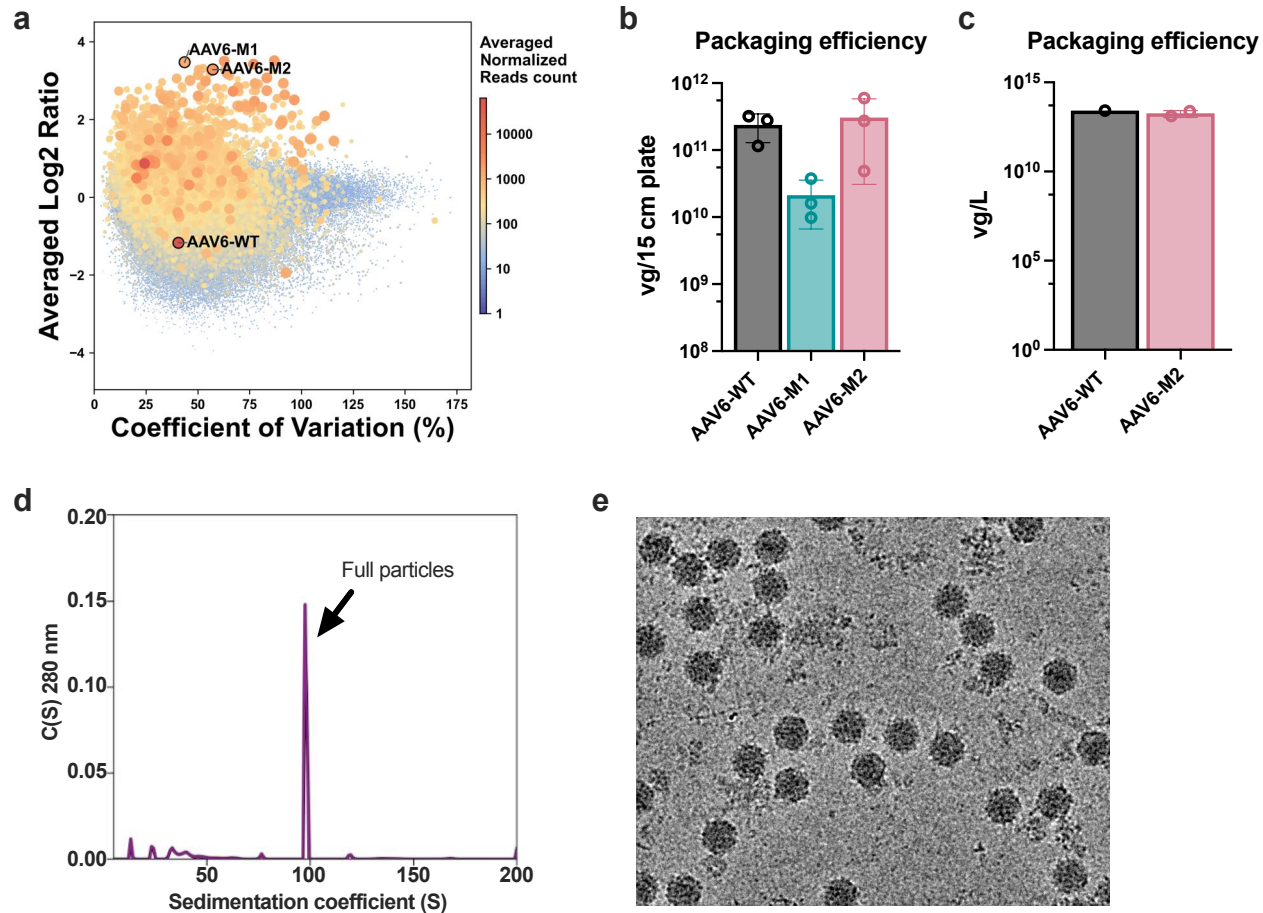
(e) Images of the livers of B6 mice 10 days post scAAV-EGFP systemic administration.

### **Supplementary Figure 7 Gating strategies**

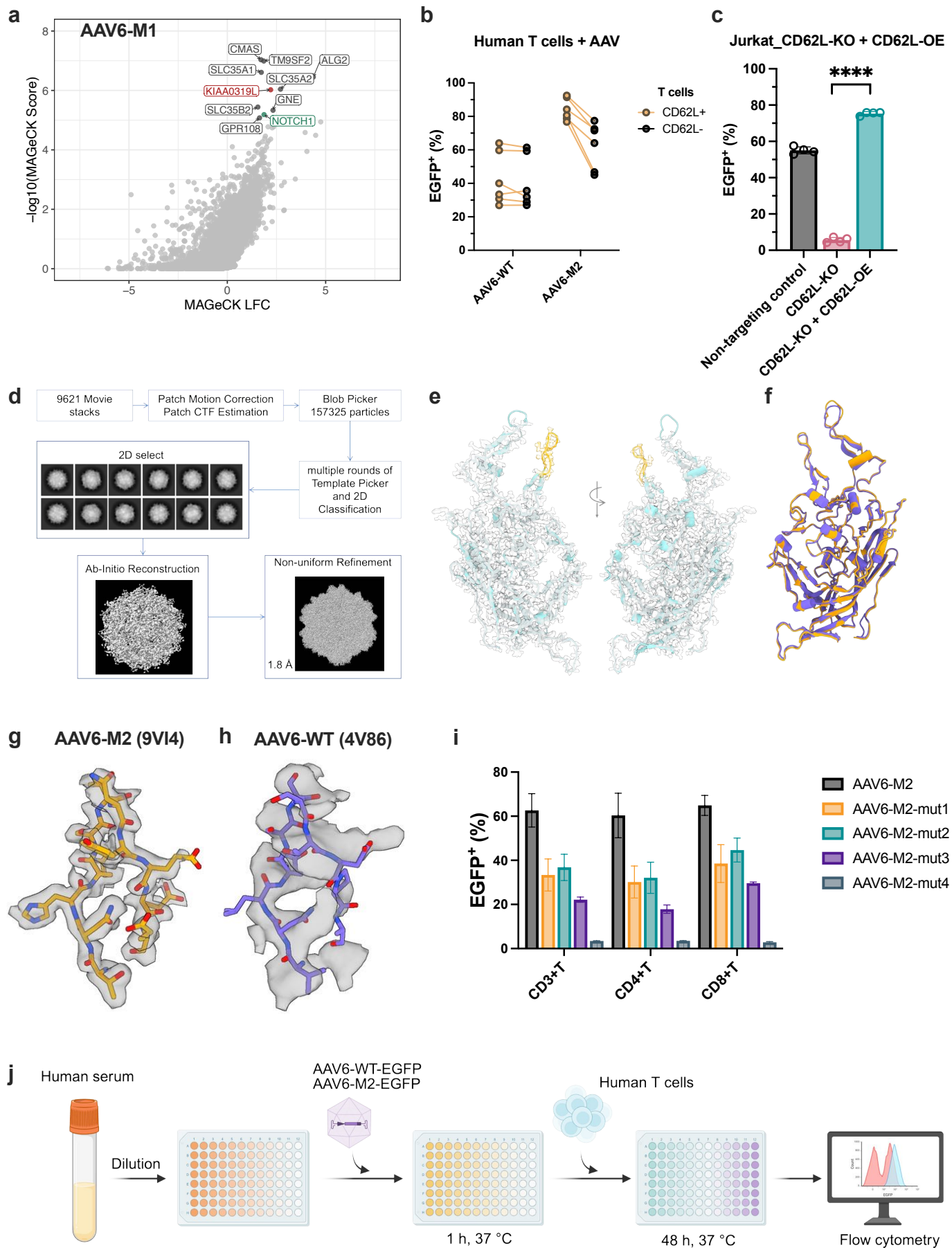
(a) Gating strategy of the HIS mouse model.

(b) Gating strategy of the HIS SLE mouse model.

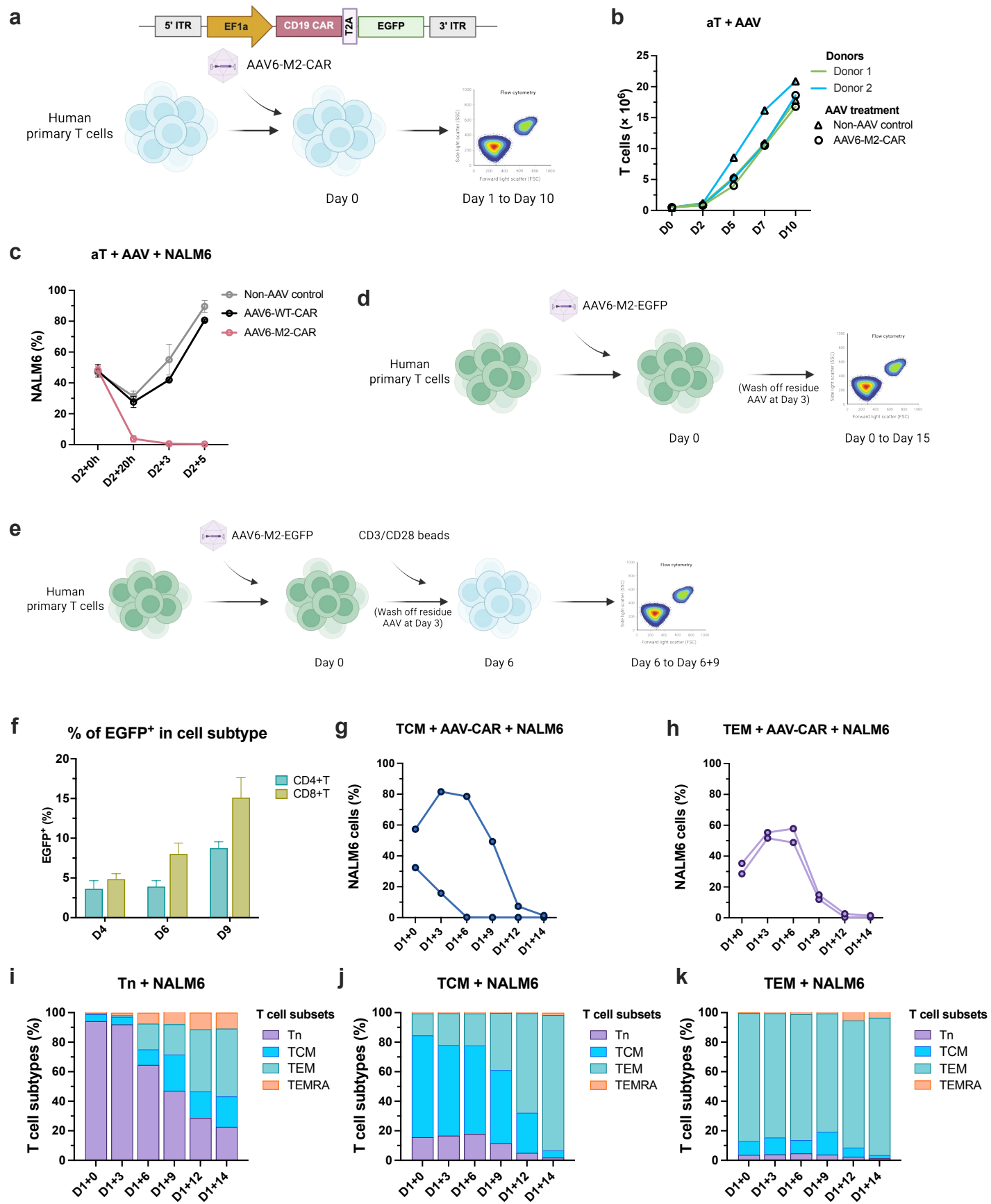
# Supplementary Figure 1



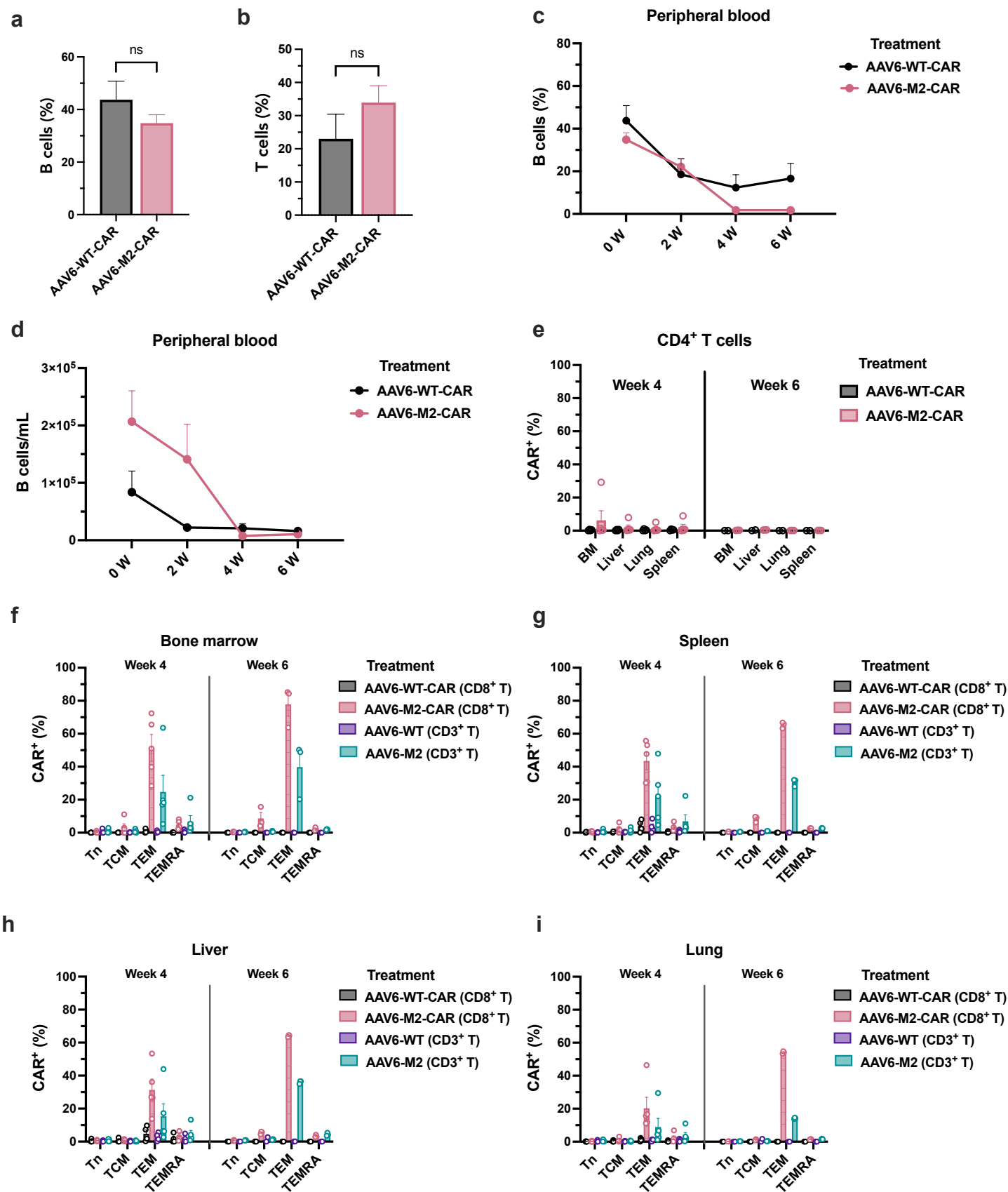
# Supplementary Figure 2



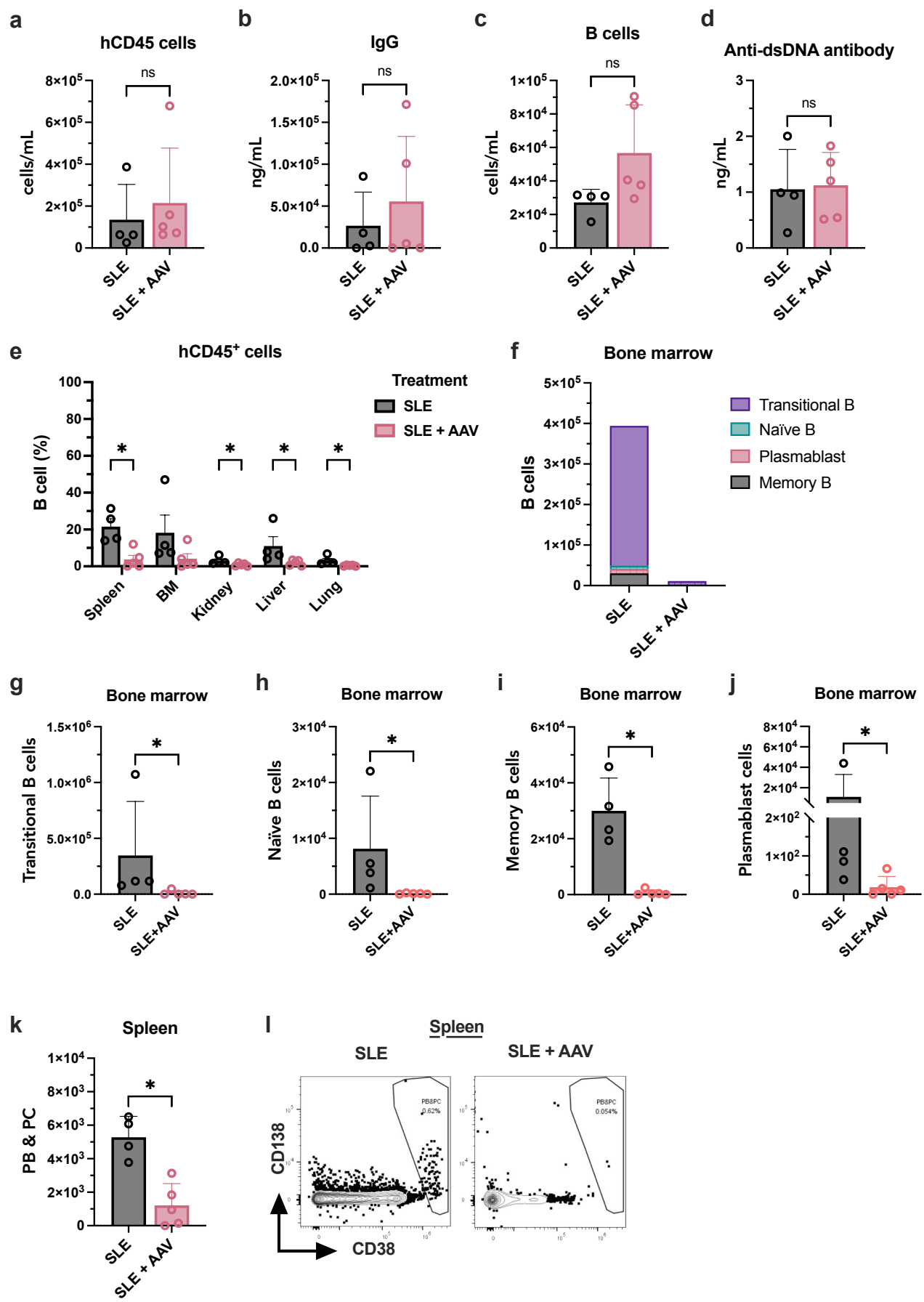
# Supplementary Figure 3



# Supplementary Figure 4



# Supplementary Figure 5



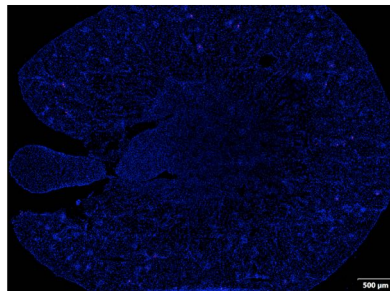
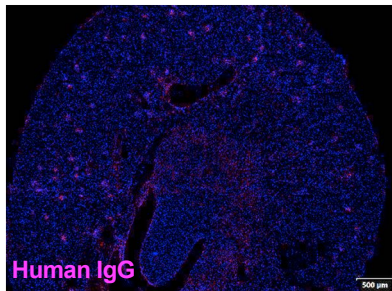
# Supplementary Figure 5 (continued)

m

Kidney

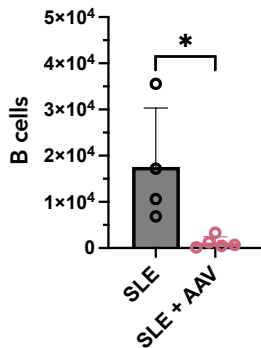
SLE

SLE + AAV



n

Lung

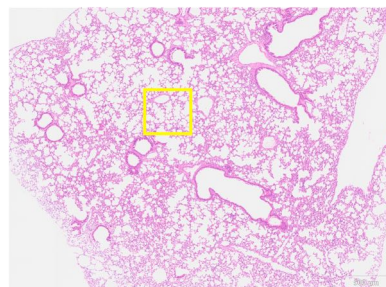
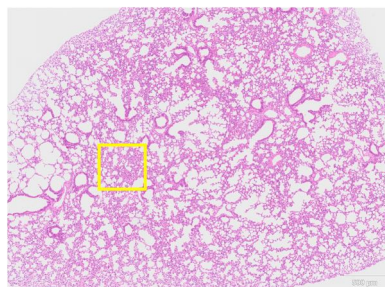


o

Lung

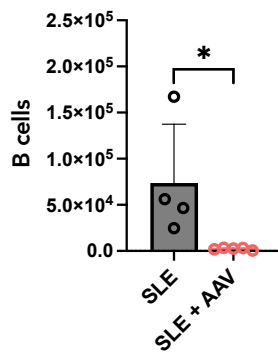
SLE

SLE + AAV



p

Liver

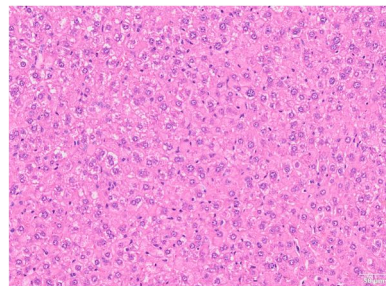
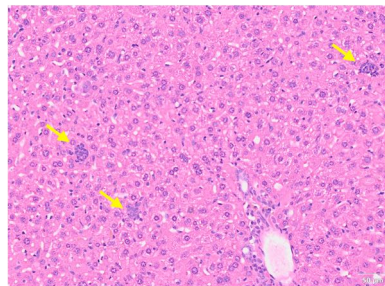


q

Liver

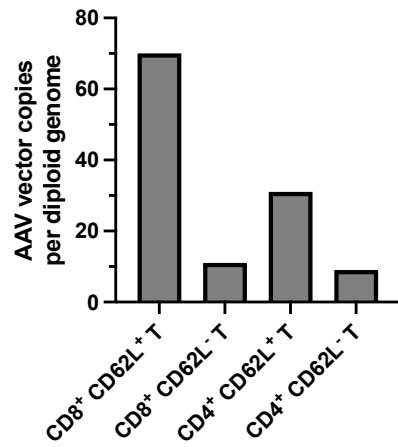
SLE

SLE + AAV

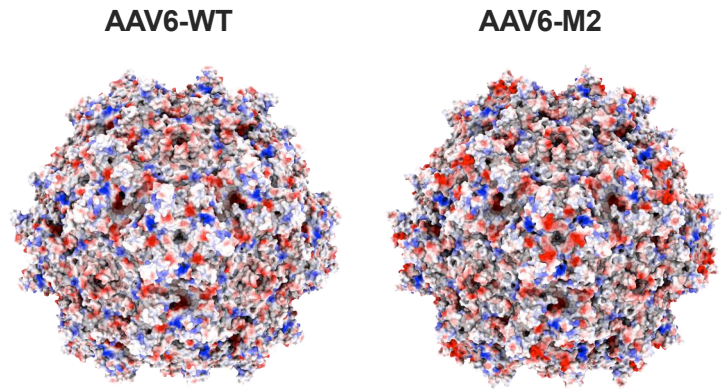


# Supplementary Figure 6

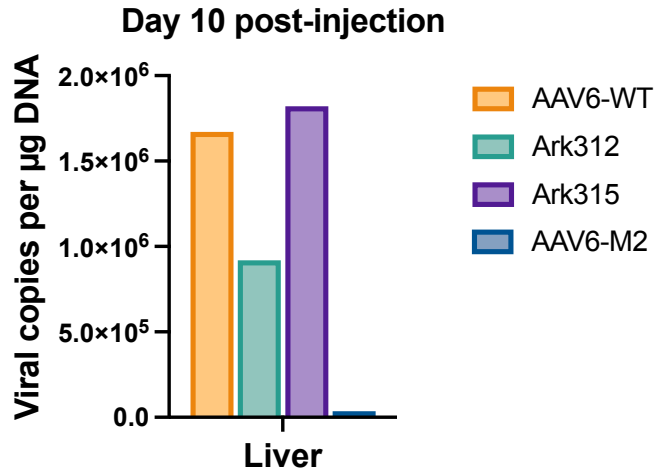
**a** Human T cells in the spleen of HIS mouse



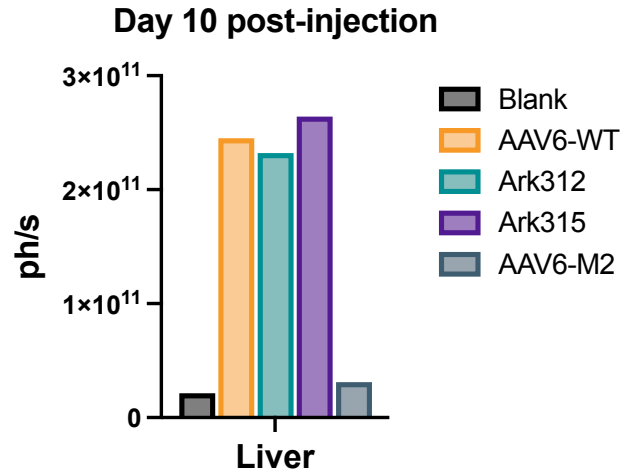
**b**



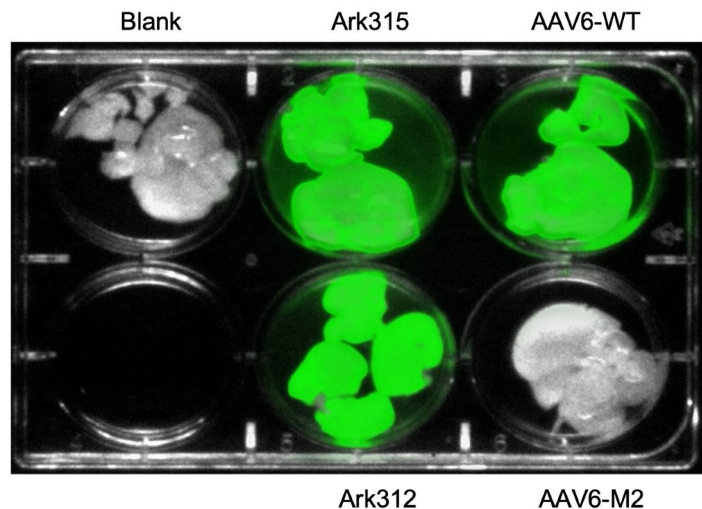
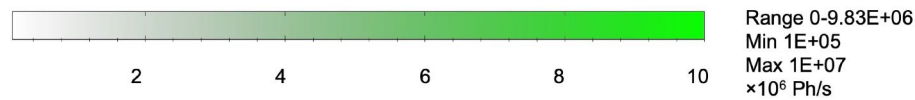
**c**



**d**

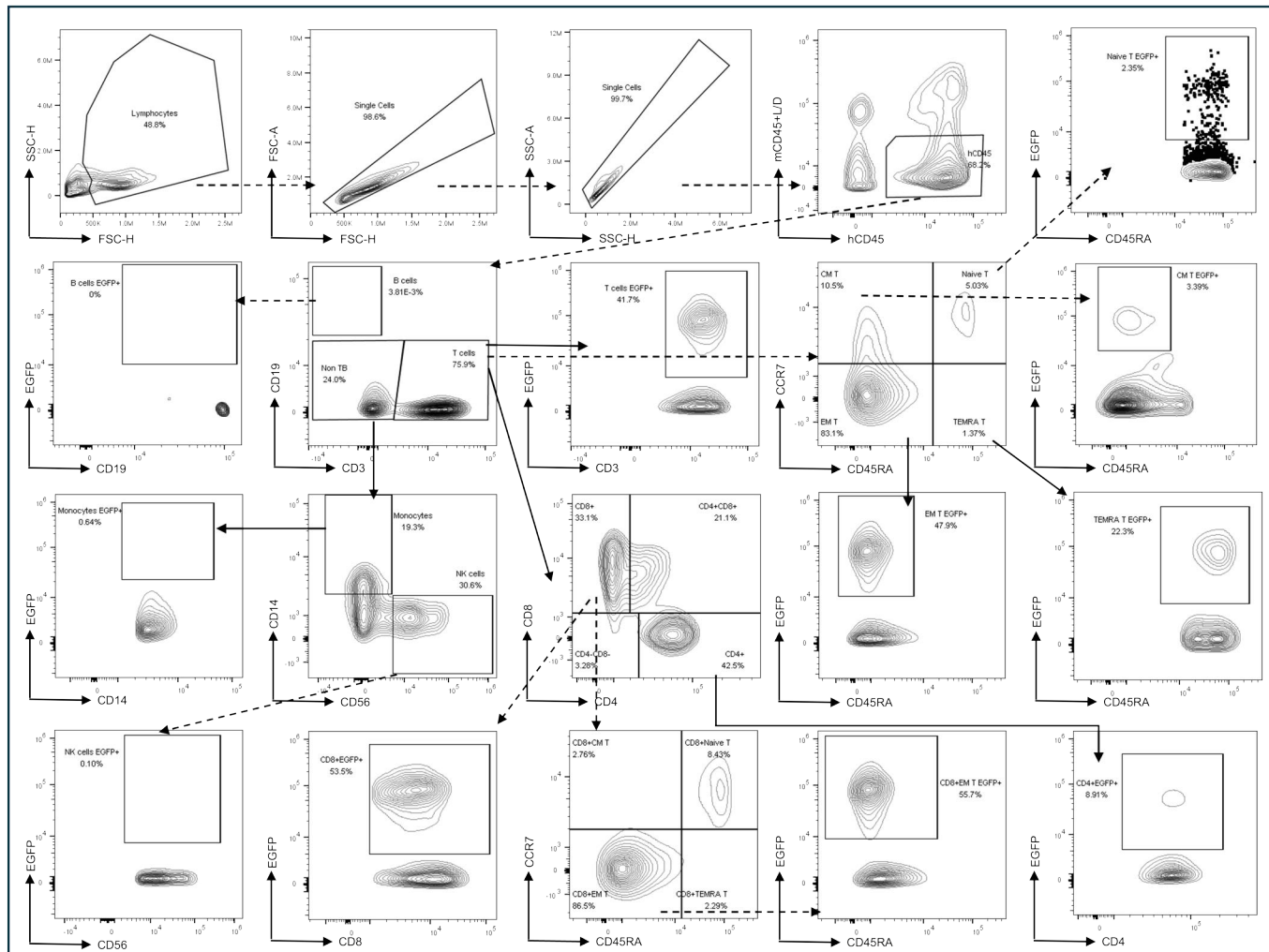


**e**



# Supplementary Figure 7

**a**



**b**

